Available online at www.sciencedirect.com
ScienceDirect
International Journal of Thermal Sciences 46 (2007) 1153–1162
International Journal of Thermal Sciences
www.elsevier.com/locate/ijts

Heat transfer characteristics of gaseous flows in micro-channel with constant heat flux

Chungpyo Hong [a,*], Yutaka Asako [a], Jae-Heon Lee [b]

[a] *Department of Mechanical Engineering, Tokyo Metropolitan University, Minami-Osawa, Hachioji, Tokyo, 192-0397, Japan*
[b] *Department of Mechanical Engineering, Hanyang University, Heangdang-dong, Sungdong-ku, Seoul, 133-791, Republic of Korea*

Received 7 June 2006; received in revised form 27 October 2006; accepted 30 October 2006

Available online 4 December 2006

Abstract

Two-dimensional compressible momentum and energy equations are solved to obtain the heat transfer characteristics of gaseous flows in parallel-plate micro-channels with CHF (constant heat flux) for no-slip regime. The numerical methodology is based on the Arbitrary-Lagrangian–Eulerian (ALE) method. The computations are performed for channels with constant heat flux which ranges from 10^2 to 10^4 W m^{-2}. The channel height ranges from 10 to 100 μm and the aspect ratio of the channel length and height is 200. The stagnation pressure, p_{stg} is chosen in such a way that the Mach number at the exit ranges from 0.1 to 0.7. The outlet pressure is fixed at the atmosphere. The heat transfer characteristics in micro-channels are obtained. And comparisons with available experimental values were conducted. The wall and bulk temperatures in micro-channels are compared with those of the incompressible flow in the conventional sized parallel plate channel. A correlation for the prediction of the wall temperature of the gaseous flow in the micro-channel is proposed. And supplementary runs with slip boundary conditions for $h = 10$ μm conducted and slip effect is discussed.

Keywords: Convective heat transfer; Gaseous flow; Micro-channel; Numerical analysis

1. Introduction

Fabrication of small devices has increased the needs for understanding of fluid flow and heat transfer in micro-geometries. Since the early work of Tuckerman [1], many experimental and numerical investigations on fluid flow and heat transfer in micro-channels have been undertaken. It is known qualitatively that gaseous flow in a micro-channel is affected by the rarefaction (the slip on the surface), the surface roughness and the compressibility effects separately or simultaneously. The compressibility effect on fluid flow characteristics has been investigated by many researchers, e.g. Prud'homme et al. [2], Berg et al. [3], Guo and Wu [4], Sayegh et al. [5] and Sun and Faghri [6]. Recently, Asako et al. [7,8] performed computational investigations on the effect of the compressibility for a wide range of *Re* and *Ma* numbers flows in parallel plate micro-channels and micro-tubes. They found that $f\,Re$ is a function of the *Ma* number in the quasi-fully developed region of both cases where the gaseous flow is accelerated. They compared their numerical results with experimental data by Turner et al. [9] and found that both results have the same tendency. As mentioned above, the fluid flow characteristics in micro-channels have been well investigated comparing with the heat transfer.

Wu and Little [10] measured the heat transfer coefficients for nitrogen flow through micro-heat exchanger. They found that Nusselt numbers are higher than those predicted by the conventional correlations for fully developed laminar and turbulent flows due to the roughened surface. Choi et al. [11] also measured heat transfer coefficient for the flow of nitrogen gas in micro-tubes for both laminar and turbulent regimes. The measured Nusselt number in the turbulent regime well exceeded the prediction for the conventional sized channel. Guo [12] performed numerical investigations on heat transfer characteristics of gaseous flow in a micro-channel for few cases. Shi et al. [13] and Miyamoto et al. [14] performed experimental investigations on fluid flow and heat transfer characteristics of the continuum

* Corresponding author. Tel.: +(81) 42 677 2711; fax: +(81) 42 677 2701.
E-mail address: cphong@comp.metro-u.ac.jp (C. Hong).

1290-0729/$ – see front matter
doi:10.1016/j.ijthermalsci.2006.10.015

Nomenclature

A	per-cycle transfer area per unit depth
C_p	specific heat
D_h	hydraulic diameter ($= 2h$)
f	Maxwell's reflection coefficient
h	channel height
	specific enthalpy
i	specific internal energy
k	thermal conductivity
Kn	Knudsen number
ℓ	channel length
$\dot{m}$	total mass flow rate per unit depth
Ma	Mach number
Nu_x	local Nusselt number
p	pressure
Pr	Prandtl number
q''	heat flux
R	gas constant
Re	Reynolds number
T	temperature
T_b	bulk temperature
$T_{b,incomp}$	bulk temperature of incompressible flow
T_k	dynamic temperature
T_w	wall temperature
$T_{w,incomp}$	wall temperature of incompressible flow
u, v	velocity components
x, y	coordinates
X^*	dimensionless axial length

Greek symbols

α	thermal accommodation coefficient
ϕ	dissipation function
γ	specific heat ratio
μ	viscosity
ρ	density
σ	molecular mean free path
τ	shear stress

Subscripts

in	inlet
out	outlet
s	slip flow
stg	stagnation value

and slip choked flows of low-dense air through a narrow parallel channel with adiabatic walls and with uniform heat flux walls, respectively. As mentioned above, investigations on heat transfer characteristics of gaseous flows in micro-chanels have been progressed gradually. However, Rostami et al. [15] reviewed the heat transfer characteristics of gas flowing in micro-channels cannot be adequately predicted by the theories and correlations developed for conventional sized channels. And, Morini [16] reviewed that further systematic studies are required to generate a sufficient body of knowledge of the transport mechanism responsible for the variation of the flow structure and heat transfer in micro-channels.

Recently, Aydin and Avci [17] investigated the effects of viscous dissipation, the velocity slip and the temperature jump at the wall on the heat transfer characteristics of gases in micropipes for a hydrodynamically and thermally fully developed flow. Ji et al. [18] performed a flow and heat transfer numerical simulation for a 2D compressible gas flow through a micro-channel in the slip regime to investigate the effects of wall roughness. They pointed out that the influence of wall roughness on the average heat transfer rate is smaller than that on the Poiseuille number. Renksizbulut et al. [19,20] investigated on incompressible gas flow and heat transfer in the entrance region of rectangular and trapezoidal micro-channels numerically in both continuum and slip flow regime. They proposed practical engineering correlations for the friction and heat transfer coefficients in those micro-channels.

In the previous study, Asako et al. [21,22] performed computational investigations on heat transfer characteristics of gaseous flow in a micro-channel and micro-tube with CWT (constant wall temperature). They proposed correlations for the prediction of heat transfer rate of gaseous flow in the micro-channel and micro-tube. However, the heat transfer characteristics of gaseous flow in parallel plate micro-channels with constant heat flux have not been investigated yet. This is the motivation of the present study to conduct numerical computations to obtain heat transfer characteristics for gaseous flow in parallel-plate channels with constant heat flux whose channel height ranges from 10 to 100 μm.

2. Formulation

2.1. Description of the problem and conservation equations

The problem is modeled as a parallel-plate channel as shown in Fig. 1 with a chamber at the stagnation temperature, T_{stg}, and the stagnation pressure, p_{stg}, attached to its upstream section. The flow is assumed to be steady, two-dimensional and laminar. The fluid is assumed to be an ideal gas. For the parallel plate channel, the governing equations can be expressed as

$$\frac{\partial \rho u}{\partial x} + \frac{\partial \rho v}{\partial y} = 0 \tag{1}$$

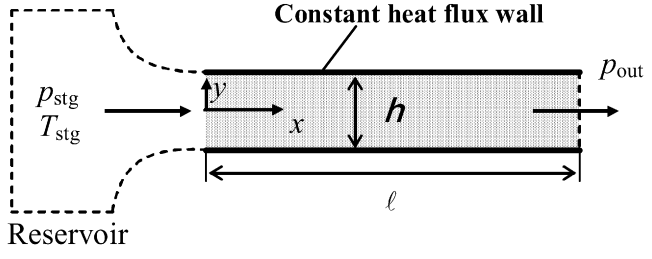

Fig. 1. A schematic diagram of problem.

$$\frac{\partial \rho uu}{\partial x}+\frac{\partial \rho uv}{\partial y}=-\frac{\partial p}{\partial x}+\mu\left(\frac{\partial^2 u}{\partial x^2}+\frac{\partial^2 u}{\partial y^2}\right)+\frac{\mu}{3}\frac{\partial}{\partial x}\left(\frac{\partial u}{\partial x}+\frac{\partial v}{\partial y}\right) \quad (2)$$

$$\frac{\partial \rho uv}{\partial x}+\frac{\partial \rho vv}{\partial y}=-\frac{\partial p}{\partial y}+\mu\left(\frac{\partial^2 v}{\partial x^2}+\frac{\partial^2 v}{\partial y^2}\right)+\frac{\mu}{3}\frac{\partial}{\partial y}\left(\frac{\partial u}{\partial x}+\frac{\partial v}{\partial y}\right) \quad (3)$$

$$\frac{\partial \rho ui}{\partial x}+\frac{\partial \rho vi}{\partial y}=-p\left(\frac{\partial u}{\partial x}+\frac{\partial v}{\partial y}\right)+k\left(\frac{\partial^2 T}{\partial x^2}+\frac{\partial^2 T}{\partial y^2}\right)+\phi \quad (4)$$

where

$$\phi=2\mu\left[\left(\frac{\partial u}{\partial x}\right)^2+\left(\frac{\partial v}{\partial y}\right)^2\right]-\frac{2\mu}{3}\left(\frac{\partial u}{\partial x}+\frac{\partial v}{\partial y}\right)^2+\mu\left(\frac{\partial u}{\partial y}+\frac{\partial v}{\partial x}\right)^2 \quad (5)$$

The equation of the state for the ideal gas is expressed by

$$i=\frac{1}{\gamma-1}\frac{p}{\rho}=\frac{R}{\gamma-1}T \quad (6)$$

The Knudsen number ($Kn=\sigma/D_h$, ratio of the gas mean free path to the characteristic length) is in the range from 3.5×10^{-5} to 3.5×10^{-3} when the channel height varies from 10 to 100 μm. If Kn is in the range from 0.001 to 0.1, the flow can be considered as a slip flow. Such slip effect leads to a reduction in the friction factor and heat transfer coefficient with increasing Kn. However, both the product of friction factor and Reynolds number ($f\,Re=96/(1+12Kn)$) and the Nusselt number are reduced only 4% when Kn is 3.5×10^{-3} [23]. The rarefaction effect is relatively insignificant when the channel height is greater than 10 μm. In the present study, the compressibility effect becomes more significant than the rarefaction effect (slip effect). Therefore, the slip on the wall is assumed to be negligible. However, the rarefaction effect (slip effect) will be discussed later.

Furthermore, with the assumptions of no slip boundary condition, uniform inlet velocity, pressure and density and specified pressure, p_{out}, at the outlet, the boundary conditions can be expressed as follows:

on the walls ($y=\pm0.5h$):

$$u=v=0,\quad -k\frac{\partial T}{\partial y}=q''\quad(\text{at } y=-0.5h)$$

$$k\frac{\partial T}{\partial y}=q''\quad(\text{at } y=0.5h)$$

at the inlet ($x=0$): $u=u_{\text{in}},\quad v=0,\quad p=p_{\text{in}},\quad \rho=\rho_{\text{in}}$

at the outlet ($x=\ell$): $p=p_{\text{out}}$ (7)

The velocity, the pressure and the density at the inlet of the channel are obtained by the stagnation treatment given by Karki [24]. The stagnation pressure can be expressed in terms of the inlet pressure, velocity and specific internal energy as follows:

$$p_{\text{stg}}=p_{\text{in}}\left[1+\frac{1}{2}\frac{u_{\text{in}}^2}{\gamma i_{\text{in}}}\right]^{\gamma/\gamma-1} \quad (8)$$

Also, from the ideal gas law, the relationship for pressure and density between stagnation and inlet point can be expressed as

$$\frac{p_{\text{stg}}}{\rho_{\text{stg}}^{\gamma}}=\frac{p_{\text{in}}}{\rho_{\text{in}}^{\gamma}} \quad (9)$$

The static pressure at the inlet can be obtained from a linear extrapolation from the interior of the computational domain. By substituting the extrapolated pressure and the stagnation pressure into Eq. (9), the inlet density is obtained. Then, using the equation of state, the specific internal energy at the inlet can be found. Finally, the inlet velocity can be determined by substituting these values into Eq. (8). The procedure is repeated until convergence is achieved.

Attention will now be focused on the calculation of the Reynolds number and Mach number that will be defined as

$$Re=\frac{2\dot{m}}{\mu}=\frac{\bar{u}D_{\text{h}}}{\mu/\bar{\rho}},\qquad Ma=\frac{\bar{u}}{\sqrt{\gamma(\gamma-1)\bar{i}}} \quad (10)$$

where the $\dot{m}$ is the mass flow and D_{h} is the hydraulic diameter. $\bar{u}$, $\bar{\rho}$ and $\bar{i}$ are the average velocity, density and specific internal energy at a cross-section

$$\bar{u}=\frac{1}{A}\int u\,\mathrm{d}A,\qquad \bar{\rho}=\int \rho u\,\mathrm{d}A\Big/\int u\,\mathrm{d}A$$

$$\bar{p}=\frac{1}{A}\int p\,\mathrm{d}A,\qquad \bar{i}=\frac{1}{\gamma-1}\frac{\bar{p}}{\bar{\rho}} \quad (11)$$

Note that the Re is constant along the channel but the Ma varies along the channel.

2.2. Numerical method

The numerical methodology is based on the Arbitrary-Lagrangian–Eulerian (ALE) method proposed by Amsden et al. [25]. The detailed description of the ALE method is documented in the literature by Amsden et al. [25] and will not be given here. The computational domain is divided into quadrilateral cells. The velocity components are defined at the vertices of the cell and other variables such as pressures, specific internal energy and density are assigned at the cell centers. The number of cells in the x-direction was 400. The cell size gradually increases in x-direction from the inlet to the mid of the channel and it gradually decreases to the exit. Since the velocity profile is almost parabolic in the semifully developed region, the number of cells in y-direction fixed at 20 for all the computations. The ALE method is a time marching method. The value of 10^{-3} was used for the convergence criterion of Newton–Raphson iteration and the convergence for the time increment was confirmed by inequalities $|\Delta\dot{m}/\dot{m}|<10^{-10}$, where $\Delta\dot{m}$ represents change in the mass flow rate, $\dot{m}$.

Supplementary runs were performed with coarse cells (100×10, 100×20) and medium cells (200×10, 200×20) to investigate the cell size effect on the results. The channel of $h=10$ μm and $\ell=2\times10^3$ μm was chosen. The values of dimensionless wall temperature at the all x-positions were examined. The computations were performed for the channel with constant heat flux of $q''=10^4$ W m^{-2} under the stagnation condition of $p_{\text{stg}}=2\times10^5$ Pa, and $T_{\text{stg}}=300$ K and with $p_{\text{out}}=10^5$ Pa.

Table 1
Effect of cell size on $(T_w - T_{in})/(q'' D_h/k)$ for $h = 10$ μm, $q'' = 10^4$ W m^{-2} and $p_{stg} = 200$ kPa

		$(T_w - T_{in})/(q'' D_h/k)$ at the outlet	Difference with fine cell (400 × 20) (%)
Coarse cells	(100 × 10)	17.204	6.1
	(100 × 20)	18.364	13.2
Medium cells	(200 × 10)	16.896	4.2
	(200 × 20)	17.417	7.4
Fine cell	(400 × 20)	16.217	–
Incompressible flow		16.12	0.6

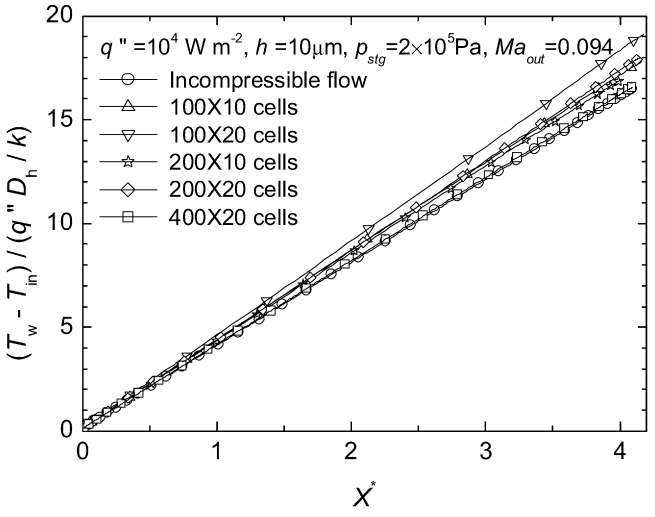

Fig. 2. Cell sizes effect on dimensionless wall temperature.

The results are tabulated in Table 1, and presented in Fig. 2. The maximum change on the dimensionless wall temperature between the coarse cells (100 × 20) and fine cells (400 × 20) at the outlet was 13.2%. As can be seen in Table 1 and Fig. 2, the change on the dimensionless wall temperature decreases with increasing the number of cell. Therefore, all the computations were performed with fine cells (400 × 20). In the case of slow flow ($Ma < 0.3$), the dimensionless wall temperature coincides with that of incompressible flow. The difference on that between the fine cells (400 × 20) and incompressible flow was 0.6%.

2.3. Comparisons with experimental data

To compare with the experimental data by Miyamoto et al. [14], the computations were performed for 4 cases whose computational conditions and channel dimensions coincide with those of the experiment. They measured local wall temperatures to obtain heat transfer characteristics of the choked flows of low-dense air through a narrow parallel channel with CHF. The inlet pressure was varied between 6.7 and 17.3 kPa and the outlet pressure was maintained to make the chocked flow. The channel length was 1.2×10^5 μm, and the height was 1×10^3 μm. Ten E-type thermocouples were embedded to the wall. T_w/T_{stg} is plotted as a function of x/L in Fig. 3 with their experimental results. The numerical results coincide well with experimental data.

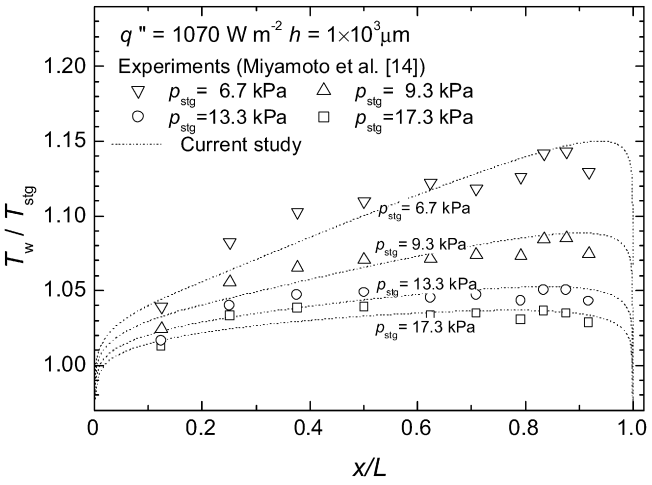

Fig. 3. T_w/T_{stg} as a function of x/L for the channel of $h = 1000$ μm and $q'' = 1070$ W m^{-2}.

3. Results and discussions

The computations were performed for the channels with the constant heat flux of $q'' = 10^2, 10^3, 10^4$ W m^{-2}. The air of $R = 287$ J (kg K)$^{-1}$, $\gamma = 1.4$, $\mu = 1.862 \times 10^{-5}$ Pa s and $\lambda = 0.0261$ W (m K)$^{-1}$ was assumed for the working fluid. The height of the channel ranges from 10 to 100 μm and the aspect ratio of the channel length and height is 200 since developing length for the incompressible flow, ℓ/D_h is 100 at $Re = 2000$. The stagnation temperature was kept at $T_{stg} = 300$ K. The stagnation pressure, p_{stg} was chosen in such a way that the Mach number at the exit ranges from 0.1 to 0.7. The outlet pressure maintained at atmospheric condition, $p_{out} = 10^5$ Pa. The channel height, the channel length, the stagnation pressure and the corresponding Reynolds and Mach numbers in the cases of $q'' = 10^3$ and 10^4 W m^{-2} are listed in Table 2. The Reynolds number obtained ranges from 10 to 3282, and the Mach number at the outlet ranges from 0.036 to 0.725 widely.

3.1. Contour plot of temperature and velocity vectors

Contour plots of the temperature for the cases of #2 ($h =$ 10 μm), #6 ($h = 10$ μm), #17 ($h = 100$ μm), and #20 ($h =$ 100 μm) are presented in Fig. 4 (a)–(d). Velocity vectors are also plotted in the figures. These are the results of $q'' = 10^4$ W m^{-2} and typical temperature contour plots for the combination of slow and fast flows in the small and large channels. The gaseous flow is accelerated in a micro-channel. Therefore, *Ma* number at the outlet is greater than that at the inlet, $Ma_{in} < Ma_{out}$. The flow whose *Ma* at the outlet is less than 0.3 is called as "slow flow" and the flow whose *Ma* at the outlet is greater than 0.3 is called as "fast flow". As can be seen in Fig. 4 (a) and (c), in the case of the slow flow ($Ma_{out} < 0.3$), the temperature rises gradually along the channel through the influence of the constant heat flux. This is the similar temperature contour to that of the incompressible flow since the temperature contour begins to develop along the channel length with parabolic curves depending on the constant heat flux. On the other hand, in the

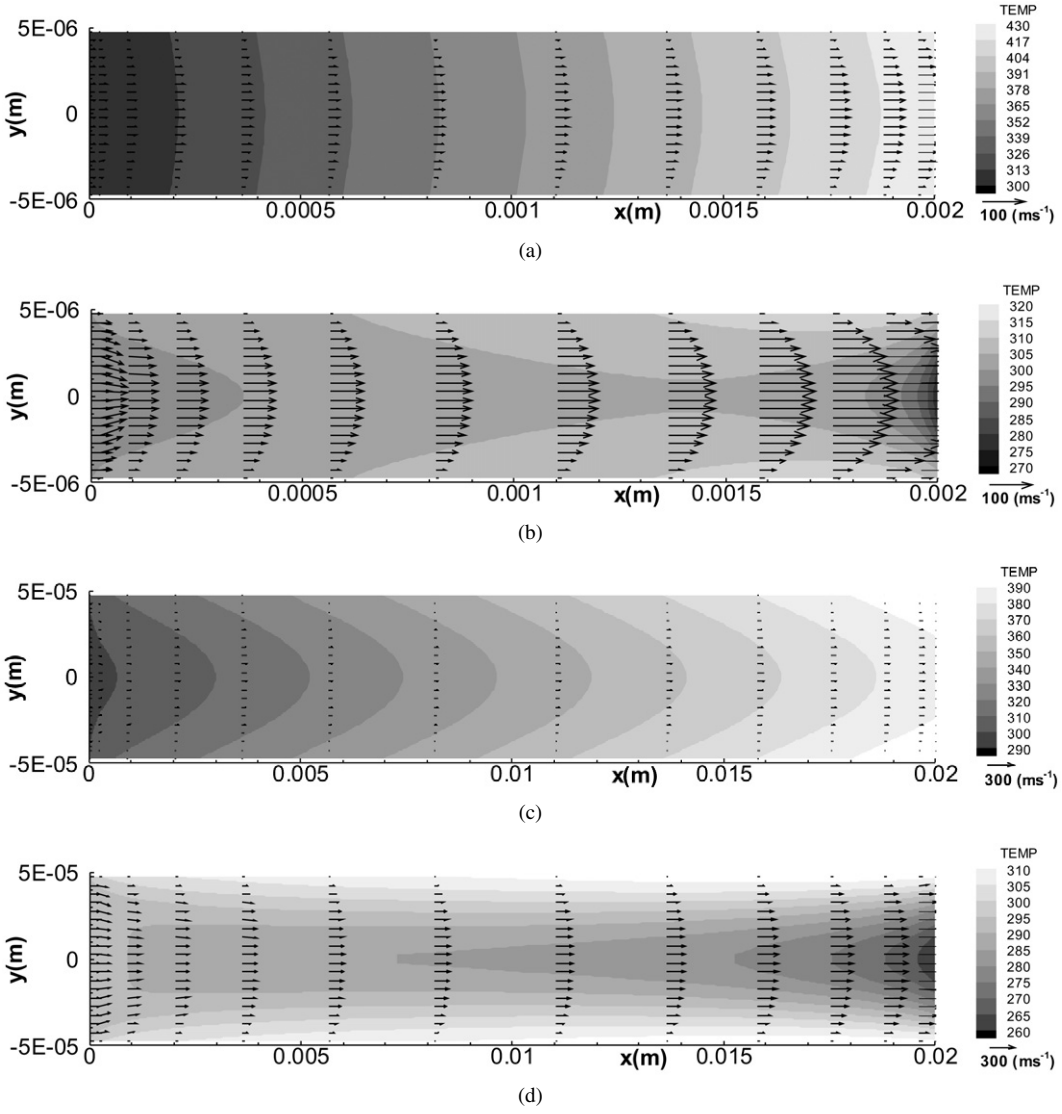

Fig. 4. Contour plots of temperature of $q'' = 10^4$ W m^{-2}. (a) #2 ($h = 10$ μm, $p_{stg} = 200$ kPa), (b) #6 ($h = 10$ μm, $p_{stg} = 600$ kPa), (c) #17 ($h = 100$ μm, $p_{stg} = 120$ kPa), (d) #20 ($h = 100$ μm, $p_{stg} = 250$ kPa).

case of the fast flow ($Ma_{out} > 0.3$), the temperature fall can be seen near the outlet due to the energy conversion into the kinetic energy caused by the flow acceleration in the core region of the channel (Fig. 4 (b) and (d)). The wall temperature decreases approaching to the outlet due to the temperature fall in the core region. This is the typical temperature contour of the compressible flow. Qualitatively similar temperature contours are also obtained for the channels with the constant heat flux of $q'' = 10^2$ and 10^3 W m^{-2}.

The value of T_w/T_{stg} for the channels of 100 μm and $q'' = 10^4$ W m^{-2} is plotted as a function of x in Fig. 5. *Ma* number is also plotted in that figure. In the case of the slow flow, T_w/T_{stg} increases along the channel linearly through the influence of constant heat flux. On the other hand, in the case of fast flow, the temperature fall can be seen near the inlet and the outlet due to the energy conversion into the kinetic energy. The wall temperature fall corresponds to the increment of the *Ma* number.

3.2. Wall temperature and Nusselt number of incompressible flow

In the case of the incompressible flow, the local Nusselt number, based on the temperature difference between the wall and the bulk temperatures, of a simultaneously developing flow in a duct with the constant heat flux is defined as

$$Nu_x = \frac{q'' D_h}{(T_w - T_b)k} \tag{12}$$

If the flow is incompressible, the bulk temperature is expressed by the function of x as

$$T_b = T_{in} + \frac{2q''x}{\int \rho C_p u \, dA} \tag{13}$$

The wall temperature of an incompressible flow in a duct is expressed as a function of a local Nusselt number and the location

Table 2
Channel height, length, p_{stg} and Re and Ma_{out}

#	h (μm)	ℓ (μm)	p_{stg} (kPa)	Re		Ma_{out}	
				$q'' = 10^3$ (W m^{-2})	$q'' = 10^4$ (W m^{-2})	$q'' = 10^3$ (W m^{-2})	$q'' = 10^4$ (W m^{-2})
1	10	2×10^3	150	17	10	0.040	0.036
2			200	41	34	0.095	0.094
3			250	70	64	0.164	0.163
4			300	106	99	0.244	0.243
5			400	190	183	0.428	0.428
6			500	287	281	0.631	0.630
7	20	4×10^3	150	67	54	0.079	0.077
8			200	157	144	0.182	0.181
9			250	263	250	0.301	0.3
10			300	380	367	0.429	0.428
11			400	636	624	0.69	0.691
12	50	1×10^4	130	242	191	0.105	0.103
13			150	389	344	0.180	0.179
14			200	814	780	0.370	0.368
15			250	1238	1205	0.55	0.548
16			300	1660	1625	0.719	0.718
17	100	2×10^4	120	540	470	0.126	0.124
18			140	1046	974	0.241	0.239
19			180	1949	1877	0.439	0.437
20			250	3354	3282	0.725	0.723

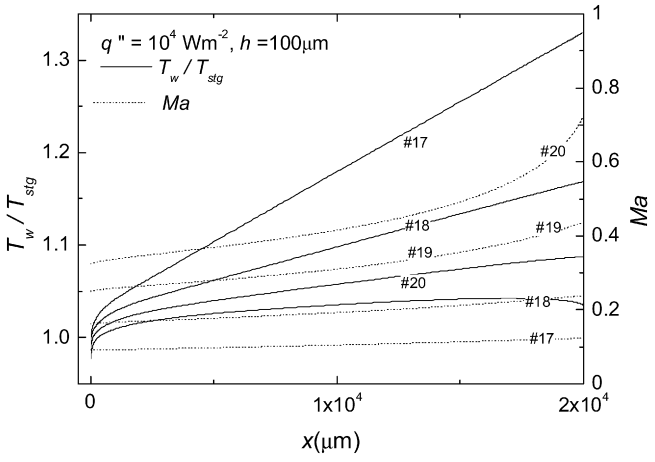

Fig. 5. T_w/T_{stg} and Ma as a function of x for $h = 100$ μm.

as

$$T_w = \left(4X^* + \frac{1}{Nu_x}\right)\left(\frac{q'' D_h}{k}\right) + T_{in} \tag{14}$$

where X^* is the inverse of Graetz number defined by

$$X^* = \frac{x}{D_h RePr} \tag{15}$$

Eq. (14) can be rewritten as

$$\frac{T_w - T_{in}}{q'' D_h/k} = 4X^* + \frac{1}{Nu_x} \tag{16}$$

The dimensionless wall temperature of an incompressible flow in a duct is a function of X^* and Nu_x. The laminar heat transfer characteristics for incompressible duct flows has been investigated by many researchers and Nusselt numbers were reported

Table 3
X^* and Nu_x (Hwang and Fan [27]) and $(T_{w,incomp} - T_{in})/(q'' D_h/k)$

Parallel plate channel ($Pr = 0.7$)		
X^*	Nu_x	$(T_{w,incomp} - T_{in})/(q'' D_h/k)$
0.000714	21.98	0.04835
0.00179	15.11	0.07334
0.00625	10.03	0.1247
0.0107	8.9	0.15516
0.0286	8.24	0.23576
0.0893	8.22	0.47863
0.143	8.22	0.69343

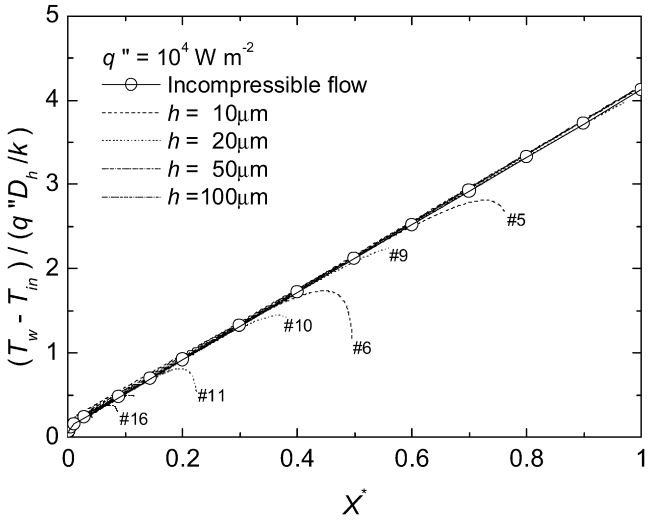

Fig. 6. Dimensionless wall temperatures as a function of X^* of $q'' = 10^4$ W m^{-2}.

in literature (e.g. Shah et al. [26]). In the case of parallel plate, the numerically obtained Nu_x for the simultaneously developing flow for $Pr = 0.7$ by Hwang and Fan [27] was used for the calculation of the wall temperature for the incompressible flow. The calculated dimensionless wall temperature for the channel is tabulated in Table 3.

3.3. Estimation of wall temperature

The dimensionless wall temperature, $(T_w - T_{in})/(q'' D_h/k)$, for the channels of $q'' = 10^4$ W m^{-2} is plotted as a function of X^* in Fig. 6. The dimensionless wall temperature for the incompressible flow (values in Table 3) is also plotted in the figure. As can be seen in Fig. 6 in the case of slow flow, the dimensionless wall temperature increases along the dimensionless length and it coincides with that of incompressible flow. On the other hand, in the case of fast flow, the dimensionless wall temperature increases gradually along the dimensionless length and level off and decreases quickly approaching to the outlet due to the conversion of the thermal energy into the kinetic energy. The qualitative same tendency can be seen for the channels with $q'' = 10^2$ and 10^3 W m^{-2}. Therefore, in the case of fast flow ($Ma_{out} > 0.3$), the wall temperature of the gaseous flow in the micro-channel cannot be directly estimated from the correlation for the incompressible flow. In addition, the computed dimensionless temperatures of several cases are slightly

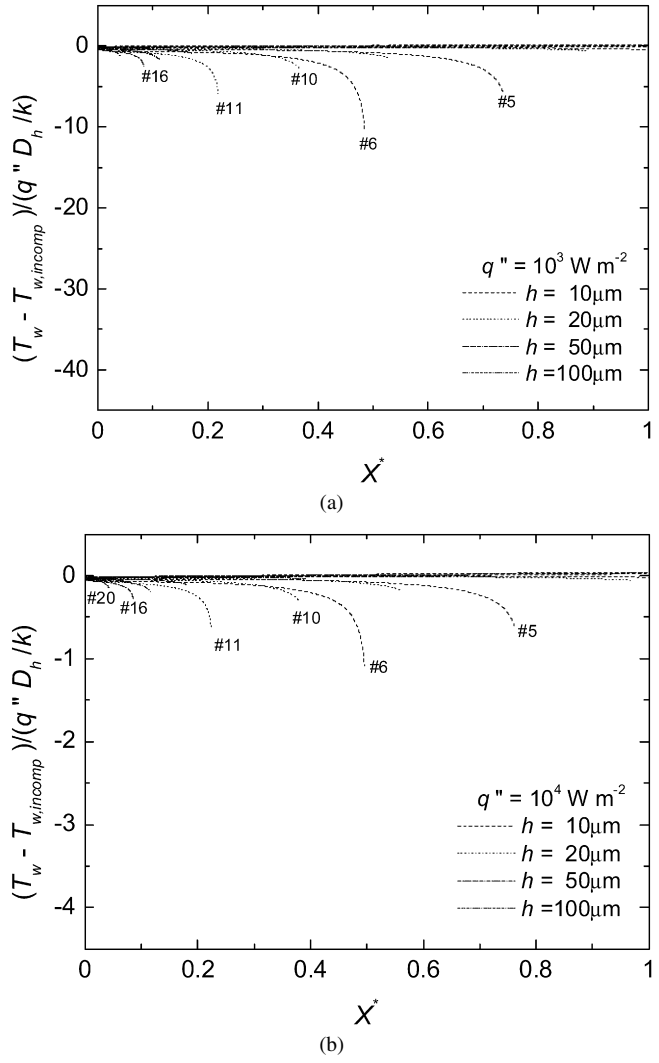

Fig. 7. Dimensionless wall temperature differences as a function of X^*. (a) $q'' = 10^3$ W m^{-2}, (b) $q'' = 10^4$ W m^{-2}.

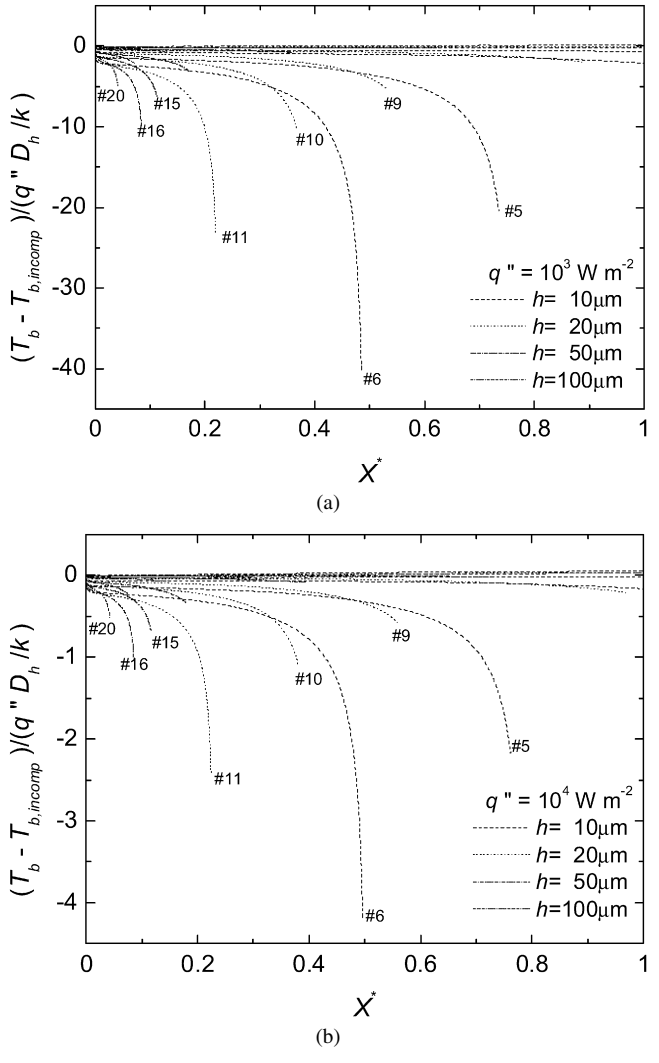

Fig. 8. Dimensionless bulk temperature differences as a function of X^*. (a) $q'' = 10^3$ W m^{-2}, (b) $q'' = 10^4$ W m^{-2}.

higher than that of the incompressible flow near the inlet since the effect of viscous dissipation is relatively prevalent before the flow acceleration occurs.

The dimensionless wall temperature differences, $(T_w - T_{w,incomp})/(q'' D_h/k)$, between the gaseous flow and incompressible flow for $q'' = 10^3$ and 10^4 W m^{-2} are plotted as a function of X^* in Fig. 7 (a) and (b), respectively. Also, the dimensionless bulk temperature differences, $(T_b - T_{b,incomp})/(q'' D_h/k)$, between the gaseous flow and incompressible flow for $q'' = 10^3$ and 10^4 W m^{-2} are plotted as a function of X^* in Fig. 8 (a) and (b), such as Fig. 7. In the case of slow flow, the dimensionless wall and bulk temperatures coincide with those of incompressible flow. Therefore, there is no difference between them as shown in Figs. 7 and 8. On the other hand, in the case of fast flow, the dimensionless wall and bulk temperature difference decreases approaching to the outlet.

Note that the bulk temperature difference between the gaseous flow and incompressible flow represents the dynamic temperature of the fluid, T_k, defined as

$$T_k = \frac{\int \rho u (u^2/2)\,dA}{\int \rho C_p u\,dA} \tag{17}$$

The gas temperature decreases near the outlet due to the energy conversion into the kinetic energy as shown in Fig. 4. If the thermal conductivity of the gas is extremely high, the wall temperature falls corresponding to the fall of the bulk temperature. However, in actual situation, the thermal conductivity of the gas is low, therefore the fall of the wall temperature is smaller than that of the bulk temperature as shown in Figs. 7 and 8. Then, the ratio of wall temperature difference between the gaseous flow and incompressible flow and the dynamic temperature, α is defined as

$$\alpha = \frac{T_{w,incomp} - T_w}{T_k} \tag{18}$$

The ratio α calculated from Eq. (18) for $q'' = 10^2$, 10^3 and 10^4 W m^{-2} is plotted in Fig. 9 as a function of the *Ma* number at the outlet. For the case of slow flow, the flow can be assumed to be an incompressible flow, and the temperature differences between the wall temperature and the wall temperature of incompressible flow and the dynamic temperature are quite small, therefore, it is not plotted in Fig. 9. The ratio α is inde-

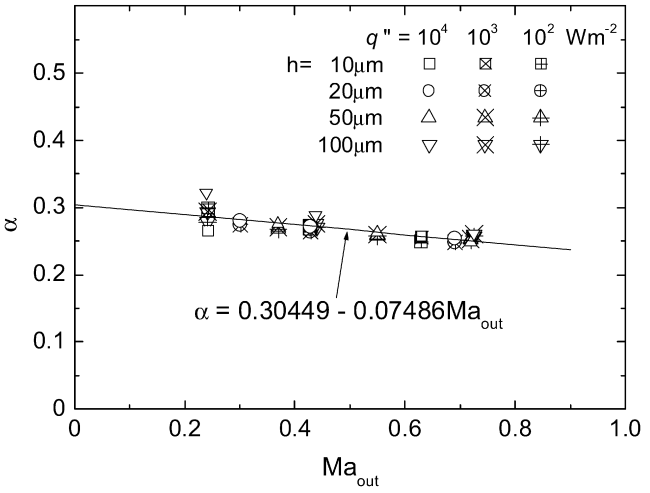

Fig. 9. α as a function of Ma_{out}.

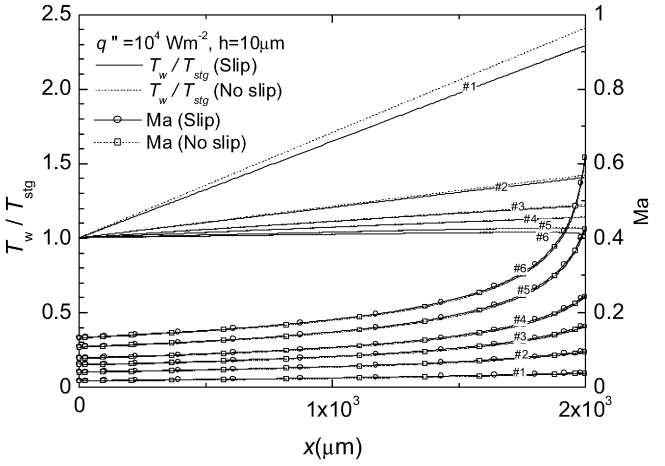

Fig. 10. $T_{\text{w}}/T_{\text{stg}}$ and Ma as a function of x for $h = 10$ μm and $q'' = 10^4\ \text{W m}^{-2}$.

pendent of heat flux and decreases with increasing the Ma at the outlet. Eq. (18) can be rewritten as

$$T_{\text{w}} = T_{\text{w,incomp}} - \alpha T_{\text{k}} \tag{19}$$

Then, the wall temperature of the channel with constant heat flux can be predicted from the wall temperature of the incompressible flow, the ratio α and the dynamic temperature. The flow characteristics under the specified stagnation and outlet pressures can be easily obtained using the correlation for $f\,Re$ and Ma obtained in our previous study [7,8].

3.4. Rarefaction effect (slip effect)

Since early analytical studies of Sparrow and Lin [28] and Inman [29], many experimental and numerical investigations on the rarefaction effect (slip effect) have been conducted. It is well known that the rarefaction effect depends on the Knudsen number and is dominant in which the characteristic length is less than 10 μm. Such rarefaction effect can be studied by solving the momentum and energy equations with the slip boundary conditions, in which the velocity slip, temperature jump, and shear stress work on the wall take into account. The slip boundary conditions only at the wall of $y = \pm h/2$ are expressed as follows [28]:

The slip velocity u_{s}

$$u_{y=\pm h/2} = u_{\text{s}} = \frac{2-f}{f}\sigma\left(\frac{\partial u}{\partial y}\right)_{y=\pm h/2} \tag{20}$$

The temperature jump

$$T_{\text{w}} = T_{y=\pm h/2} - \frac{2-a}{a}\frac{2\gamma}{\gamma+1}\frac{\sigma}{Pr}\left(\frac{\partial T}{\partial y}\right)_{y=\pm h/2} \tag{21}$$

The shear stress work

$$k\left(\frac{\partial T}{\partial y}\right)_{y=\pm h/2} = -q'' - \mu u_{\text{s}}\left(\frac{\partial u}{\partial y}\right)_{y=\pm h/2} \tag{22}$$

where σ is the mean free path, f is Maxwell's reflection coefficient and a is a thermal accommodation coefficient.

Table 4
Channel height, length, $p_{\text{stg}}Re$, Ma, and Kn of $q'' = 10^4\ \text{W m}^{-2}$ for slip regime

#	h (μm)	ℓ (μm)	p_{stg} (kPa)	Re	Ma_{in}	Ma_{out}	Kn_{in}	Kn_{out}
1	10	2×10^3	150	9	0.017	0.039	0.0023	0.0052
2			200	33	0.041	0.097	0.0017	0.0041
3			250	64	0.061	0.167	0.0014	0.0038
4			300	99	0.078	0.248	0.0011	0.0036
5			400	182	0.108	0.434	8.6×10^{-4}	0.0035
6			500	280	0.133	0.638	6.9×10^{-4}	0.0033

Also Kn number can be expressed as [30]

$$Kn = \frac{\sigma}{D_{\text{h}}} = \sqrt{\frac{\pi\gamma}{2}}\frac{Ma}{Re} \tag{23}$$

In the present study, the Knudsen number is in the range from 3.5×10^{-5} to 3.5×10^{-3} when the channel height varies from 10 to 100 μm. Therefore, the supplementary computation was conducted to investigate on the slip effect with slip boundary conditions for limiting cases of $h = 10$ μm and $q'' = 10^4\ \text{W m}^{-2}$. The channel height, the channel length, the stagnation pressure and the corresponding Re, Ma and Kn numbers in those cases are listed in Table 4. As can be seen in Eq. (23) and Table 4, the rarefaction effect is dominant for lower Re, however, the compressibility effect is significant with increasing Ma for higher Re.

Attention will be turn to the influence of slip flow on the heat transfer, the values of $T_{\text{w}}/T_{\text{stg}}$ and Ma for the channel are plotted as a function of x in Fig. 10. The results obtained in the no slip boundary condition are also plotted in the figure. Ma number of the slip conditions coincides well with that of the no slip conditions. For the #1 case ($Ma_{\text{out}} = 0.039$), the maximum difference in $T_{\text{w}}/T_{\text{stg}}$ between slip and no slip boundary conditions at the outlet is 4%. On the other hand, for the #2–6 cases, the difference reduces less than 1%. Consequently, with increasing Ma number, the compressibility effect is more dominant and the slip effect is relatively insignificant where Kn number is less than $Kn = 0.0052$.

3.5. Magnitude of viscous dissipation and compressibility terms

Expressing in terms of enthalpy using the thermodynamics relations, $h = i - p/\rho$, Eq. (4) can be rewritten as

$$\frac{\partial \rho u h}{\partial x} + \frac{\partial \rho v h}{\partial y} = \left(u\frac{\partial p}{\partial x} + v\frac{\partial p}{\partial y} \right) + k\left(\frac{\partial^2 T}{\partial x^2} + \frac{\partial^2 T}{\partial y^2} \right) + \phi \tag{24}$$

The first term on the right-hand side of Eq. (24) is called as the compressibility effect by Bejan [31]. For the ideal gas, Eq. (24) can be expressed by

$$C_p\left(\frac{\partial \rho u T}{\partial x} + \frac{\partial \rho v T}{\partial y} \right) = \left(u\frac{\partial p}{\partial x} + v\frac{\partial p}{\partial y} \right) + k\left(\frac{\partial^2 T}{\partial x^2} + \frac{\partial^2 T}{\partial y^2} \right) + \phi \tag{25}$$

By neglecting viscous dissipation (V. D.) and compressibility effect (C. E.) terms, Eq. (25) can be rewritten as

$$C_p\left(\frac{\partial \rho u T}{\partial x} + \frac{\partial \rho v T}{\partial y} \right) = k\left(\frac{\partial^2 T}{\partial x^2} + \frac{\partial^2 T}{\partial y^2} \right) \tag{26}$$

The Nusselt number in Table 3 for the incompressible flow was obtained by Hwang and Fan [27] solving Eq. (26), respectively. However, in the present work, the viscous dissipation and compressibility effect terms are included in the calculation as shown in the energy equation. In the case of slow flow, temperature curves almost coincide with those of incompressible flow as shown in Figs. 6, 7, and 8. Therefore, the supplementary computation for the case of fast flow, #6 was conducted neglecting V. D. term and/or C. E. term. The dimensionless wall temperature obtained for #6 of $q'' = 10^4\ \mathrm{W\,m^{-2}}$ is plotted as a function of X^* in Fig. 11. The results of compressible and incompressible flow are also plotted in the figures. The dimensionless wall temperatures obtained by neglecting both V. D. and C. E. terms almost coincide with those of incompressible flow. In the case of neglecting only C. E. term, the wall temperature increases gradually due to the failure of absorption of V. D. energy generated near the wall. Therefore, the dimensionless wall temperature is higher than that of incompressible flow. On the other hand, in the case of neglecting only V. D. term, the dimensionless wall temperature is lower than that of incompressible flow due to flow acceleration in the core region of the channel. Also, dimensionless wall temperature fall can be seen near the outlet due to temperature fall through C. E. As a result of that, the dimensionless wall temperature of compressible flow is slightly higher than that of incompressible flow along the channel due to V. D., however, it is slightly lower than that of incompressible flow near the outlet due to C. E. The dimensionless wall temperature difference between neglecting only V. D. or C. E. term and incompressible flow is considerable. It is note worthy that the dimensionless wall temperature of compressible flow is very close to the temperature obtained by neglecting V. D. and C. E. terms although the Mach number at the outlet reaches about 0.63.

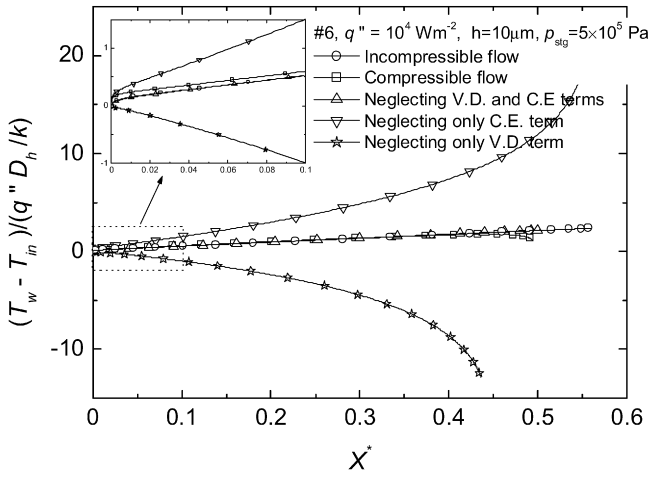

Fig. 11. Effect of viscous dissipation and compressibility terms on dimensionless wall temperature.

4. Concluding remarks

Two-dimensional compressible momentum and energy equations are solved to obtain the heat transfer characteristics of gaseous flow in a micro-channel with CHF. The following conclusions are obtained.

(1) In the case of slow flow, the identical temperature profiles normalized by heat flux are obtained with those of incompressible flow. However, in the case of fast flow in a micro-channel, different temperature profiles are obtained.
(2) The wall temperature of a micro-channel can be predicted from the wall temperature of the incompressible flow, the ratio α and the dynamic temperature.

$$T_w = T_{w,\mathrm{incomp}} - \alpha T_k$$

(3) With increasing *Ma* number, the compressibility effect is more dominant and the slip effect is relatively insignificant when the channel height ranges from 10 to 100 μm.

Acknowledgements

Financial support from the Japan Society for the Promotion of Science (Grant-in-aid for Scientific Research (C) #16560189) is greatly acknowledged.

References

[1] D.B. Tuckerman, R.F.W. Pease, High-performance heat sinking for VLSI, IEEE Electron Device Lett. EDL-2 (5) (1981) 126–129.
[2] R.K. Prud'homme, T.W. Chapman, J.R. Bowen, Laminar compressible flow in a tube, Appl. Sci. Res. 43 (1986) 67–74.
[3] H.R. Berg, C.A. Seldam, P.S. Gulik, Compressible laminar flow in a capillary, J. Fluid Mech. 246 (1993) 1–20.
[4] Z.Y. Guo, X.B. Wu, Compressibility effect on the gas flow and heat transfer in a micro tube, Int. J. Heat Mass Transfer 40 (13) (1997) 3251–3254.
[5] R. Sayegh, M. Faghri, Y. Asako, B. Sunden, Direct simulation Monte Carlo of gaseous flow in micro-channel, in: Proceedings of the ASME National Heat Transfer Conference, August 15–17, 1999, Albuquerque, NM.

[6] H. Sun, M. Faghri, Effect of rarefaction and compressibility of gaseous flow in micro channel using DSMC, Numer. Heat Transfer Part A 38 (1999) 153–158.
[7] Y. Asako, T. Pi, S.E. Turner, M. Faghri, Effect of compressibility on gaseous flows in micro-channels, Int. J. Heat Mass Transfer 46 (2003) 3041–3050.
[8] Y. Asako, K. Nakayama, Effect of compressibility on gaseous flows in micro-tube, in: Proceedings of the ASME 2003 National Heat Transfer Conference, July 21–23, 2003, Las Vegas, NV, USA.
[9] S.E. Turner, L.C. Lam, M. Faghri, O.J. Gregory, Experimental investigation of gas flow in micro-channels, J. Heat Transfer 126 (2004) 753–763.
[10] P. Wu, W.A. Little, Measurement of the heat transfer characteristics of gas flow in fine channel heat exchangers used for microminiature refrigerators, Cryogenics 24 (1984) 415–420.
[11] S.B. Choi, R.F. Barron, R.O. Warrington, Fluid flow and heat transfer in micro tubes, in: Micro Mechanical Sensors, Actuators and Systems, ASME DSC, vol. 32, Atlanta, GA, 1991, pp. 123–134.
[12] Z.Y. Guo, Size effect on flow and heat transfer characteristics in MEMS, in: Proceedings of the International Conference on Heat Transfer and Transport Phenomena in Microscale, October 15–20, 2000, Banff, Canada.
[13] W. Shi, M. Miyamoto, Y. Katoh, J. Kurima, Choked flow of low density gas in a narrow parallel-plate channel with adiabatic wall, Int. J. Heat Mass Transfer 44 (2001) 2555–2565.
[14] M. Miyamoto, W. Shi, Y. Katoh, M. Kodama, Choked flow and heat transfer of rarefied gas in a narrow parallel-plate channel with uniformly heating walls, Int. J. Heat Mass Transfer 46 (2003) 2685–2693.
[15] A.A. Rostami, A.S. Mujumdar, N. Saniei, Flow and heat transfer for gas flowing in micro-channels: A review, Heat and Mass Transfer 38 (2002) 359–367.
[16] G.L. Morini, Single-phase convective heat transfer in micro-channels: a review of experimental results, Int. J. Thermal Sci. 43 (2004) 631–651.
[17] O. Aydin, M. Avci, Heat and fluid flow characteristics of gases in micropipes, Int. J. Heat Mass Transfer 49 (2006) 1723–1730.
[18] Y. Ji, K. Yuan, J.N. Chung, Numerical simulation of wall roughness on gaseous flow and heat transfer in a micro-channel, Int. J. Heat Mass Transfer 49 (2006) 1329–1339.
[19] M. Renksizbulut, H. Niazmand, Laminar flow and heat transfer in the entrance region of trapezoidal channels with constant wall temperature, J. Heat Transfer 128 (2006) 63–74.
[20] M. Renksizbulut, H. Niazmand, G. Tercan, Slip-flow and heat transfer in rectangular micro-channels with constant wall temperature, Int. J. Thermal Sci. 45 (9) (2006) 870–881.
[21] Y. Asako, H. Toriyama, Heat transfer characteristics of gaseous flows in micro-channels, Microscale Thermophys. Eng. 9 (2005) 15–31.
[22] Y. Asako, Heat transfer characteristics of gaseous flows in a micro-tube, Thermal Sci. Eng. 12 (5) (2004) 31–37.
[23] E.K. George, A. Beskok, Micro Flow Fundamentals and Simulation, Springer, New York, 2001, pp. 151–158.
[24] K.C. Karki, A calculation procedure for viscous flows at all speeds in complex geometries, PhD thesis, University of Minnesota, Minneapolis, 1986.
[25] A.A. Amsden, H.M. Ruppel, C.W. Hire, SALE a simplified ALE computer program for fluid flow at all speeds, Los Alamos Scientific Lab Rep., LA-8095, Los Angeles, 1980.
[26] R.K. Shah, A.L. London, Laminar Flow Forced Convection in Ducts, Advances in Heat Transfer, Academic Press, New York, 1978.
[27] C.L. Hwang, L.T. Fan, Finite difference analysis of forced-convection heat transfer in entrance region of a flat rectangular duct, Appl. Sci. Res. Sect. A 13 (1964) 401–422.
[28] E.M. Sparrow, S.H. Lin, Laminar heat transfer in tubes under slip-flow conditions, J. Heat Transfer 84 (4) (1962) 363–369.
[29] R.M. Inman, Laminar slip flow heat transfer in a parallel-plate channel or a round tube with uniform wall heating, NASA TD-2393, 1964.
[30] H.P. Kavehpour, M. Faghri, Y. Asako, Effects of compressibility and rarefaction on gasous flows in micro-channels, Numer. Heat Transfer Part A 32 (1997) 677–696.
[31] A. Bejan, Convection Heat Transfer, second ed., Wiley, New York, 1995, pp. 11–14.